Finite Element Simulation of Three Full-Scale Crash Tests for Cessna 172 Aircraft*

Brian H. Mason† and Jerry E. Warren, Jr. ‡

NASA Langley Research Center, Hampton, VA, 23681-2199

The NASA Emergency Locator Transmitter Survivability and Reliability project was initiated in 2013 to assess the crash performance standards for the next generation of emergency locator transmitter (ELT) systems. Three Cessna 172 aircraft were acquired to perform crash testing at the NASA Langley Research Center Landing and Impact Research Facility. Full-scale crash tests were conducted in the summer of 2015 and each test article was subjected to severe, but survivable, impact conditions including a flare-to-stall during emergency landing, and two controlled-flight-into-terrain scenarios. Finite element analyses were performed to numerically simulate the aircraft response to the crash tests. The first test simulated impacting a concrete surface represented analytically by a rigid plane. Tests 2 and 3 simulated impacting a dirt surface represented analytically by an Eulerian grid of brick elements using a Mohr-Coulomb material model. The objective of this paper is to summarize the test and analysis results for the three full-scale crash tests. Simulation models of the airframe which correlate well with the tests are needed for future studies of alternate ELT mounting configurations.

*Previously presented at the 2017 AIAA Science and Technology (SciTech) Forum and Exposition in Grapevine, TX on 9-13 January 2017 as AIAA Paper 2017-0631 https://doi.org/10.2514/6.2017-0631.
†Research Aerospace Engineer, Structural Mechanics and Concepts Branch, Mail Stop 190, AIAA Associate Fellow
‡Research Aerospace Engineer, Structural and Thermal Systems Branch, Mail Stop 431, Member AIAA

I. Introduction

A. Motivation and Background

In 2013, the NASA Search and Rescue (SAR) Mission Office at Goddard Space Flight Center (GSFC) initiated a study to assess the crash performance standards of the next generation of emergency locator transmitters (ELT). SAR is particularly interested in ensuring that ELTs are not mounted in locations in which ELTs or their wired antenna connections will be damaged during a crash. In pursuit of this ELT-SAR study, three Cessna 172 aircraft were acquired by NASA and subjected to severe, but survivable crash tests in the summer of 2015. The crash tests enable evaluation of ELT performance under conditions that more accurately replicate actual crash environments than those found in the current performance standard [1]. Each aircraft was equipped with four to five ELTs. These crash tests were conducted at the Landing and Impact Research (LandIR) [2 and 3] facility at NASA Langley Research Center (LaRC). A photo of the LandIR is shown in Fig. 1. The details of the test set up and rigging are documented in another reference [4]. The data from the three tests were used to calibrate structural finite element (FE) models of the airframes. Once calibrated, these models can be used to predict the airframe and ELT responses at various aircraft impact conditions. The analyses will lead to updated installation standards for the entire ELT system (beacon, antenna, and interconnecting cabling).

Fig. 1. NASA Landing and Impact Research (LandIR) facility.

Beginning in the mid-1970s, the LandIR facility at LaRC was used for testing general aviation (GA) aircraft for improved crashworthiness [5 to 13]. Data from tests conducted between 1974 and 1983 were used to assist the Federal Aviation Administration (FAA) in establishing seat certification standards [14]. The Advanced General Aviation Transport Experiments (AGATE) program was established in the late 1990s as a collaboration between government and industry to revive the GA market. Full-scale crash tests of a Beech Starship in 1995 and a modified

Lancair aircraft in 2001 were performed as technology demonstrations for AGATE [15 and 16]. LandIR is a unique facility [17] that is well suited for performing the general aviation aircraft crash tests planned by the ELT-SAR project.

The Cessna 172 Skyhawk is a four-seat, single engine, high-wing airplane, manufactured by the Cessna Aircraft Company. More Cessna 172s have been built than any other aircraft and the first production models were delivered in 1956. These aircraft were selected for this series of crash tests for their availability and because ELT installation and setup do not vary significantly in aluminium alloy general aviation airframes. It is also noted that NASA had previously conducted a series of crash tests using C-172 aircraft in the 1970s [9 and 18], and these tests helped guide the development of the lifting hardware used in the current tests.

B. Objective

The purpose of this paper is to correlate explicit dynamic FE simulation models with data from the experimental tests. Correlation of the models includes comparison of airframe weight, center of gravity, kinematic response, delta-velocity (or rebound velocity), and accelerometer data between the simulation model and the experimental tests. Simulation models that represent the kinematic response of the airframe well can then be used to evaluate alternative ELT mounting configurations. Additionally, this work serves as an example for simulation of ground impact landings for other classes of aircraft including transport-category aircraft [19 and 20] as well as newer urban air mobility (UAM) class vehicles.

C. Test Description

The three Cessna high-wing, four seat, GA airplanes used for this test series are shown in Fig. 2. Test article 1 was a 1958 C-172. Test article 2 was a 1958 C-175, which is built on the C-172 airframe, but contains a different engine and gearbox. The third test article was a 1975 C-172M. Test articles 1 and 3 were operational until the winter of 2014 before their purchase by LaRC.

Test article 1 Test article 2 Test article 3

Fig. 2. ELTSAR crash test articles.

Each aircraft was outfitted with similar instrumentation, cameras, and onboard experiments. Although only one ELT is required in a GA aircraft, for testing purposes, multiple ELTs were mounted into the cabin or tail section of each aircraft for the evaluation of their performance. The rear seats and luggage area equipment were removed from each airplane, and an onboard data acquisition system (DAS) was installed in their place. The DAS recorded accelerations throughout the fuselage at a sampling rate of 10 kHz. A frame assembly was constructed on the top of the wing for rigging the airframe to the LandIR facility. Further information about the instrumentation and rigging hardware for the tests is presented in a paper by Littel [4].

All tests were conducted within the approximate landing stall speed of the aircraft. Test 1 was designed to simulate a flare-to-touchdown onto a rigid surface (concrete). This case provided a way to isolate the airframe response for model calibration. Tests 2 and 3 were designed to simulate controlled-flight-into-terrain (CFIT) conditions, where the terrain response must also be accounted for in the models. Test 2 featured the airplane impacting with a nose down attitude, while Test 3 featured the airplane impact with a nose up attitude resulting in tail strike. Tests 2 and 3 impacted a dirt surface consisting of a clay-sand mixture known as Gantry Unwashed Sand (GUS) [21]. This soil was used as the impact surface for the Transport Rotorcraft Airframe Crash Testbed (TRACT) full-scale tests [22]. Preliminary analytical results for the three crash tests were previously presented [23]. Analytical results from LS-DYNA[§] simulations were previously reported for crash tests 1 [24] and 2 [25]. The as-measured impact conditions are presented in Table 1 where the horizontal and vertical directions are defined as normal and parallel to the ground, respectively.

[§] The use of trademarks or names of manufacturers in this report is for accurate reporting and does not constitute an official endorsement, either expressed or implied, of such products or manufacturers by the National Aeronautics and Space Administration.

Table 1. Crash conditions at impact.

Test	Surface	Vertical Velocity, in./s (ft/min)	Horizontal Velocity, in./s (kts)	Pitch Angle, deg	Pitch Rate. deg/s
1	Concrete	276.0 (1380)	722.4 (35.7)	+1.48	+16.5
2	GUS	344.4 (1722)	823.2 (40.6)	-12.20	+16.1
3	GUS	283.2 (1416)	682.8 (33.7)	+8.0	+13.1

II. Model Geometry and Loads

In this section, the computer models used to simulate the impact tests are described. The derivation of the geometry for the models is described first. Next, material properties for the model are discussed. In the third part of this section, the FE model mesh representation is described.

A. Geometry for Analytical Models

Development of the FE models was complicated by the fact that no prior geometry or static load models of the C-172 airframe existed and no engineering drawings were available. Consequently, an original computer aided design (CAD) geometry of the airframe was generated using both a three-dimensional laser scan and hand measurements of the test article. The measurements were used as inputs to the Conceptual Design Shop (CDS) tool [26], an airframe geometry generation tool developed within the PATRAN FE modeling software [27]. Initial geometry from CDS was tuned to match the point cloud from the laser scan, as shown in Fig. 3. The CDS-generated geometry included internal structure (ribs, spars, frames, etc.) of the airframe. The FE model was discretized from this geometry, although several additional structural components (ELTs, point-masses, LandIR mounts) were added later.

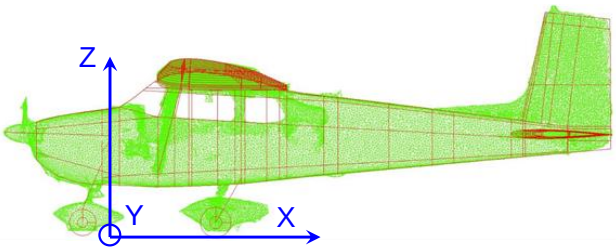

Fig. 3. CDS geometry (red) and laser scanned data (green) for C-172 airframe.

Simulations for the Test 1 and 2 configurations used the same C-172 FE airframe model. For the Test 3 C-172M airframe, the fuselage aft of frame 108 was replaced with the swept tail geometry with a rear window and narrower aft fuselage section, as shown in Fig. 4.

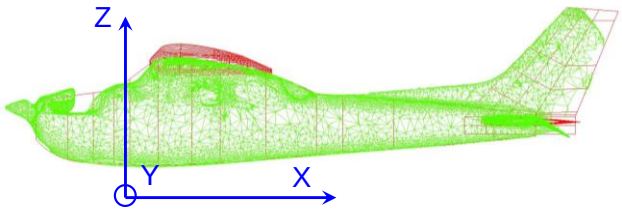

Fig. 4. CDS geometry (red) and laser scanned data (green) for C-172M airframe.

B. Material Properties

Due to the lack of data from the manufacturer, the exact material properties and component dimensions (thicknesses, beam heights, rod diameters, etc.) were unknown. Because of the large number of components in the aircraft, extensive strength and stiffness testing of all components in the aircraft was not practical, so material properties commonly used in aircraft were assumed as shown in Table 2. A magnet was used to determine that the engine mounts, landing gear, and firewall contained ferric steel; all other metallic components were assumed to be constructed of aluminum alloys. The engine and DAS boxes were not modeled in detail, but their average densities were tuned to match the measured weight. A series of hand measurements were taken of the panel thicknesses at key locations in the aircraft (forward fuselage, aft fuselage, rib, spar, and wing covers, etc.). The shock absorber in the nose landing gear is represented by a slot connector element using the load displacement curve shown in Fig. 5. The shock absorber properties in Fig. 5 were derived from measurements of the test aircraft. The first point in Fig. 5 represents the shock absorber displacement under aircraft weight. For the second point, the shock absorber is assumed to be fully compressed when 1.9 times the gross take-off weight (GTOW) of the aircraft is supported entirely by the nose wheel.

Table 2. Material elastic properties.

Material	Elastic Modulus, Msi	Poisson's Ratio, ν	Mass Density, $lb_f\ s^2/in.^4$	Yield Stress, ksi
Steel	30.0	0.300	7.359×10^{-4}	90.0
Aluminum	10.0	0.300	2.525×10^{-4}	40.0
Rubber	0.357	0.323	2.588×10^{-4}	15.0
Glass	0.500	0.300	1.124×10^{-4}	n/a

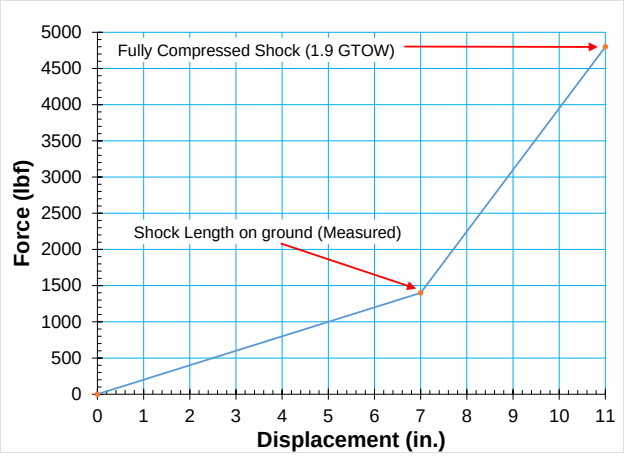

Fig. 5. Derived load-displacement curve for nose landing gear shock.

Final tuning of the mass of the computer models to the actual aircraft was accomplished through the use of point-masses. For Test 1, four point-masses (totaling 220 lb_f) were added to the model to match the weight and center of gravity (CG) of the test article, as shown in Table 3. The global coordinate system for the model is shown in Fig. 3. The Test 2 configuration is heavier than Test 1, and two point-masses (totaling 321 lb_f) were added to the model to match the weight and CG of the test article, as shown in Table 4. For Test 3, four point-masses (totaling 393 lb_f) were added to the model to match the weight and CG of the test article, as shown in Table 5.

Table 3. Test and analysis values of inertial properties for Test 1.

Parameter	Test	Model	Difference	% Diff
Weight, lb_f	2000.000	2000.013	0.013	0.001
CG_x, in.	44.500	44.500	0.000	0.000
CG_y, in.	0.000	-0.028	-0.028	n/a
CG_z, in.	46.250	46.428	0.178	0.385

Table 4. Test and analysis values of inertial properties for Test 2.

Parameter	Test	Model	Difference	% Diff
Weight, lb_f	2114.000	2113.986	-0.014	-0.001
CG_x, in.	39.500	39.500	0.000	0.000
CG_y, in.	0.000	-0.088	-0.088	n/a
CG_z, in.	48.100	48.100	0.000	0.00

Table 5. Test and analysis values of inertial properties for Test 3.

Parameter	Test	Model	Difference	% Diff
Weight, lb_f	2072.000	2071.980	-0.020	-0.001
CG_x, in.	42.500	42.500	0.000	0.001
CG_y, in.	0.000	0.073	0.073	n/a
CG_z, in.	50.800	50.601	-0.199	-0.392

C. Analysis Models

All FE analyses are performed with the Abaqus software, a product of Simulia [28]. The Abaqus model representing the Test 1 configuration is shown in Fig. 6. A nominal shell element edge length of 1.5-in. was used. This model contains 71,514 nodes, 235 beam elements, 74,640 shell elements, 400 solid elements, 66 multi-point constraints, four different materials, four revolute connectors (wheel axles), and 22 concentrated masses. The concrete impact surface was modeled as a horizontal rigid shell element, and the aircraft was set at an initial position 0.1 in. above that surface. All shell elements were defined as Abaqus S3R and S4R elements, and beam elements were defined with Abaqus B31 elements. The four ELTs, DAS box, and tires were modeled as C3D8 solid elements. The engine, seats, dummy occupants, and fuel in the wing were simulated as concentrated masses. The model required 4.5 hours of wall clock time on an 8-processor Windows 7 workstation using Abaqus/Explicit version 6.14 to simulate 0.30-seconds of impact.

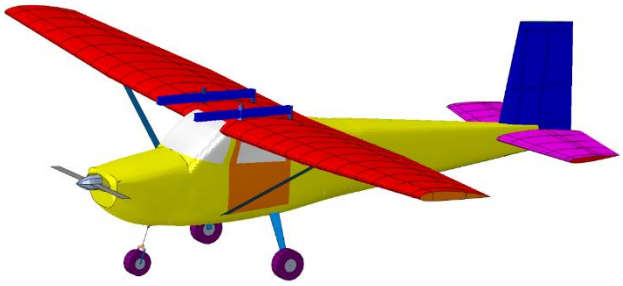

Fig. 6. Abaqus model of C-172 airframe (Test 1 and 2).

The Abaqus model representing the Test 2 configuration is identical to the Test 1 configuration with the following exceptions. First, the number and position of the ELTs (five instead of four) is different. Second, the nose landing gear shock in the test article was damaged and locked in place; so, the spring shock used to represent the landing gear in Test 1 is replaced with a 1-in.-long rigid beam. This beam is set up to break when the bending moment exceeds 240,000 lb_f-in. to simulate failure of the nose gear observed during the test. And finally, the impact surface in Test 2 is soil (30-in. deep), which is modeled in Abaqus with an Eulerian grid of 63,000 eight-node brick elements measuring 4-in. long by 3-in. wide by 2.5-in. deep. Soil properties are represented with the Mohr-Coulomb plasticity model with a density of 1.86×10^{-4} lb_f-s^2/$in.^4$ and a friction angle of 30 degrees. The model required 20 hours of wall clock time on an 8-processor Windows 7 workstation using Abaqus/Explicit version 6.14 to

simulate 0.30-seconds of impact, which is noticeably higher than the Test 1 runtime due to the additional soil elements and contact with the soil.

The Abaqus model representing the Test 3 configuration is shown in Fig. 7. A nominal shell element edge length of 1.5-in. was used. This model contains 68,133 nodes, 331 beam elements, 69,064 shell elements, 976 solid elements, 42 multi-point constraints, eight materials, four revolute connectors (wheel axles), and 24 concentrated masses. Major components (wing, fuselage, empennage, landing gear, etc.) are represented with the same types of elements as described for Test 1. The impact surface in Test 3 is soil (30-in. deep), which is modeled in Abaqus with 95,040 eight-node brick elements measuring 4-in. long by 3-in. wide by 2.5-in. deep and uses the same properties as given for Test 2. Rigid pins connecting the forward and aft fuselage are set up to break when the tensile reaction forces exceed 1000 lb_f. For all analyses, nodal location-, velocity-, and acceleration-time histories at accelerometer locations were extracted from the results file.

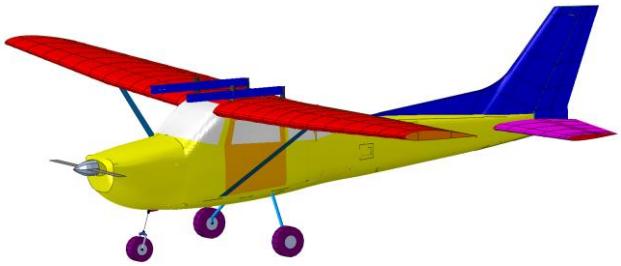

Fig. 7. Abaqus model of C-172M airframe (Test 3).

III. Test and Analysis Correlation

In this section, the results of FE simulations of crash Tests 1, 2, and 3 are presented and compared with experimental data. All three numerical models were calibrated after the experimental tests. The calibration process included minor improvements to the modeling of the landing gear due to mass and stiffness uncertainties. Initial conditions for the numerical models (test article velocities, pitch angle, and pitch rate) were matched to the observed test values as provided in Table 1..

A. Crash Test 1

A sequence of photographs taken from a high-speed camera is shown in Fig. 8, along with corresponding views of the matching model kinematics. Overall, the simulation matches the gross kinematics of the test well; the

difference in the tail impact was only about 0.01 sec. Pitch angle from photogrammetry during the test and simulation is plotted against time in Fig. 9. Simulation data were collected at the accelerometers, and the closest accelerometer to the CG (where photogrammetry data were collected) is installed on the pilot floor.

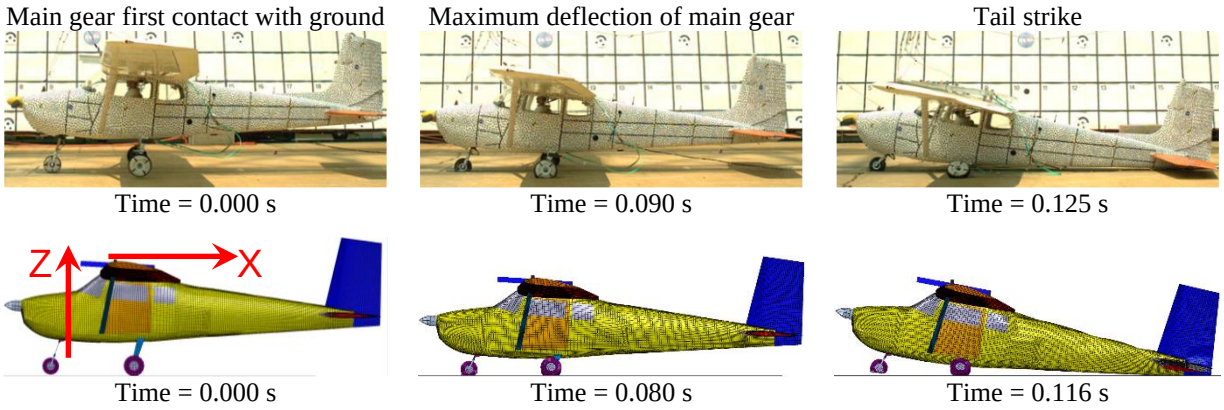

Fig. 8. Photographic images and computational results at critical kinematic events for Test 1.

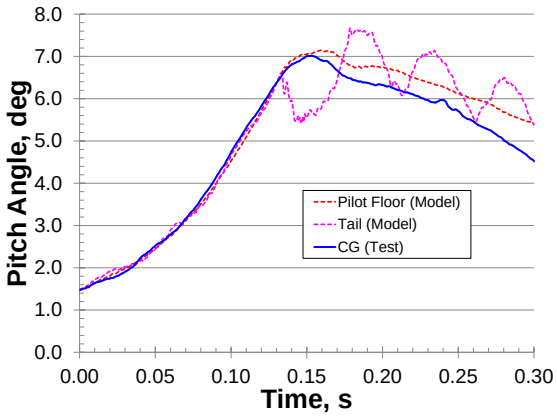

Fig. 9. Pitch angle from test and simulation against time for two locations in Test 1.

Comparisons of test and analysis results of the rebound velocity (difference between impact velocity and minimum velocity, delta-velocity), average acceleration, and peak acceleration in the vertical (Z) direction at several locations in the airframe are presented in Table 6. Only vertical accelerations are presented as the horizontal accelerations were low. Comparisons in the vertical (Z) direction are presented for three selected locations in the airframe (left door frame, DAS box, and rear bulkhead) in Fig. 10. Test and analytical acceleration data are filtered using an SAE Channel Filter Class (CFC) 20 low-pass filter [29]. Acceleration data are presented in the local reference frame (moves with aircraft as shown in Fig. 3) of each accelerometer. Velocities are presented in the

global coordinate system (shown in Fig. 8). Analytical accelerations and velocities are computed in the fixed global coordinate system. For comparison with test data, the analytical accelerations are translated into the moving local coordinate system. The photogrammetry data used to compute the pitch angles in Fig. 9 are used to transform the accelerometer data into the fixed coordinate system; these transformed accelerations are integrated to produce velocity time histories for the test.

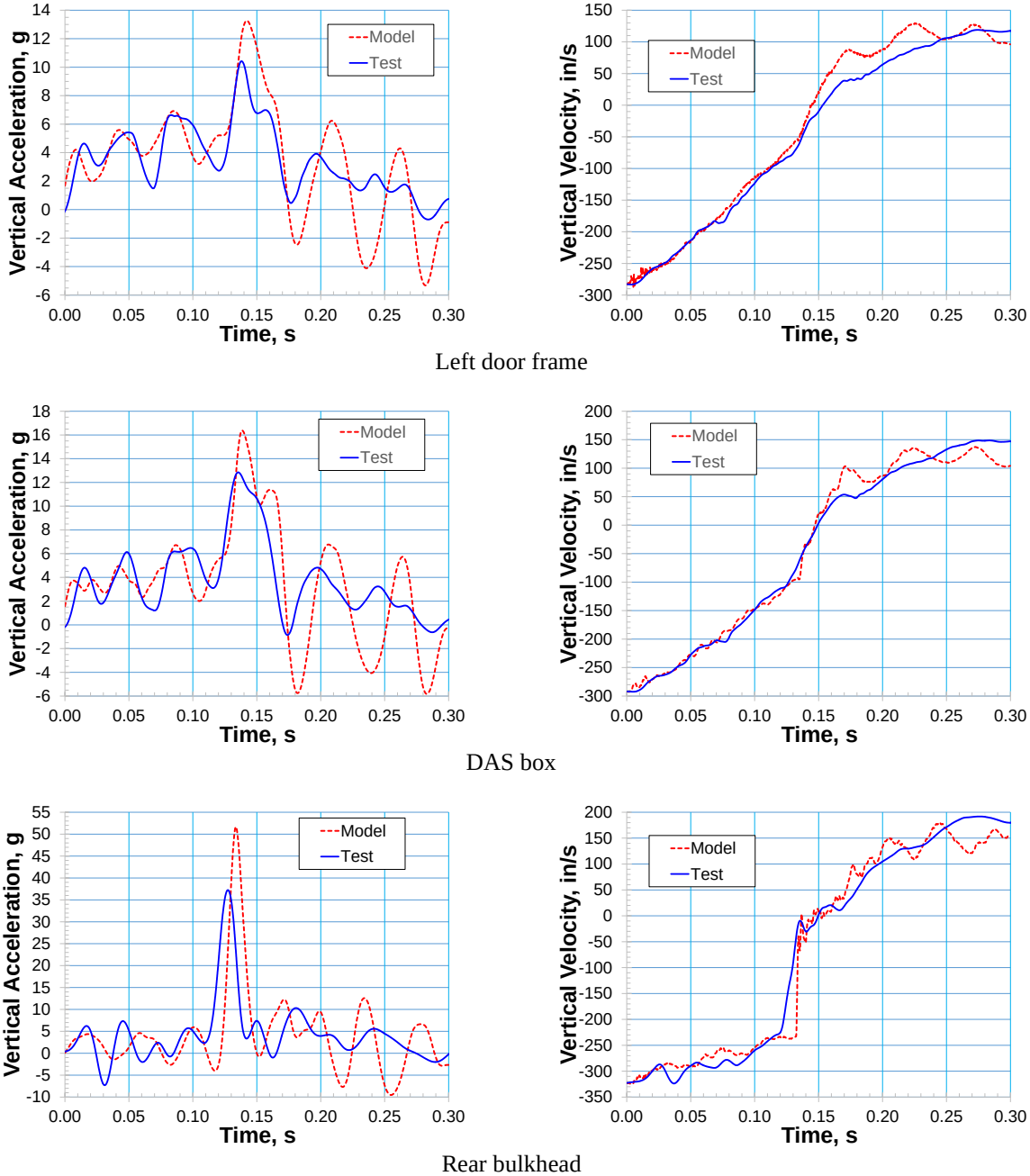

Fig. 10. Test and analysis results of local vertical acceleration and global vertical velocity in Test 1.

Table 6. Comparison of test and analysis of vertical velocity and acceleration at several locations for Test 1.

	Average Acceleration, g			Peak Acceleration, g			Delta-Velocity, in./s		
	Test	**Model**	**% Diff**	**Test**	**Model**	**% Diff**	**Test**	**Model**	**% Diff**
Pilot Z	3.5	3.9	11.5	7.6	11.4	50.1	398.0	394.6	-0.9
Copilot Z	3.7	3.8	2.4	7.2	10.5	44.4	388.5	394.1	1.4
Left Door Z	3.8	4.0	4.9	10.4	13.3	27.4	401.7	410.1	2.1
Right Door Z	3.8	4.0	7.6	10.8	12.7	17.4	426.3	407.9	-4.3
DAS Z	4.2	4.0	-2.6	12.9	16.4	27.4	440.5	429.2	-2.6
Rear Bulkhead Z	4.8	5.4	12.1	37.2	51.7	38.7	514.5	503.2	-2.2
Ceiling Z	3.8	4.0	4.8	9.8	17.8	81.3	414.0	416.6	0.6
Firewall Z	3.9	4.1	4.6	8.7	8.4	-3.8	377.0	373.9	-0.8

Test and analysis comparisons of the delta-velocity and average accelerations in the airframe are excellent; but comparisons are generally poor for the peak accelerations. Contributors to the difference in the test and simulated accelerations include uncertainties in the timing of events and the analytically perfectly rigid impact surface. Peak accelerations are also significantly affected by uncertainties in component thicknesses and weight distributions (which could not be easily measured) and lack of detail in modeling components in the vicinity of the accelerometers (such as the DAS box, the unmodeled seats, and unmodeled anthropomorphic test dummies).

B. Crash Test 2

A sequence of photographs taken from the high-speed camera is shown in Fig. 11, along with corresponding views of the matching model kinematics. Note that the simulation model is cut in half (along the XZ-symmetry plane) to show the internal structure and the nose gear soil penetration. Pitch angle from photogrammetry during the test and simulation is plotted against time in Fig. 12. The simulation predicts a nose-down rotation of the aircraft at 0.03 seconds after impact, about 0.10 seconds earlier than the rotation occurs in the test. Buckling of the aft tail section also occurs significantly earlier in the simulation than in the test; however, the rate of bending of the aft tail section after initiation of buckling is similar. In the test, the airframe maintains an almost constant pitch angle for 0.12 seconds after impact, suggesting that the modeled soil may be too stiff and is causing the nose gear of the model to dig in and flip the aircraft sooner than in the test.

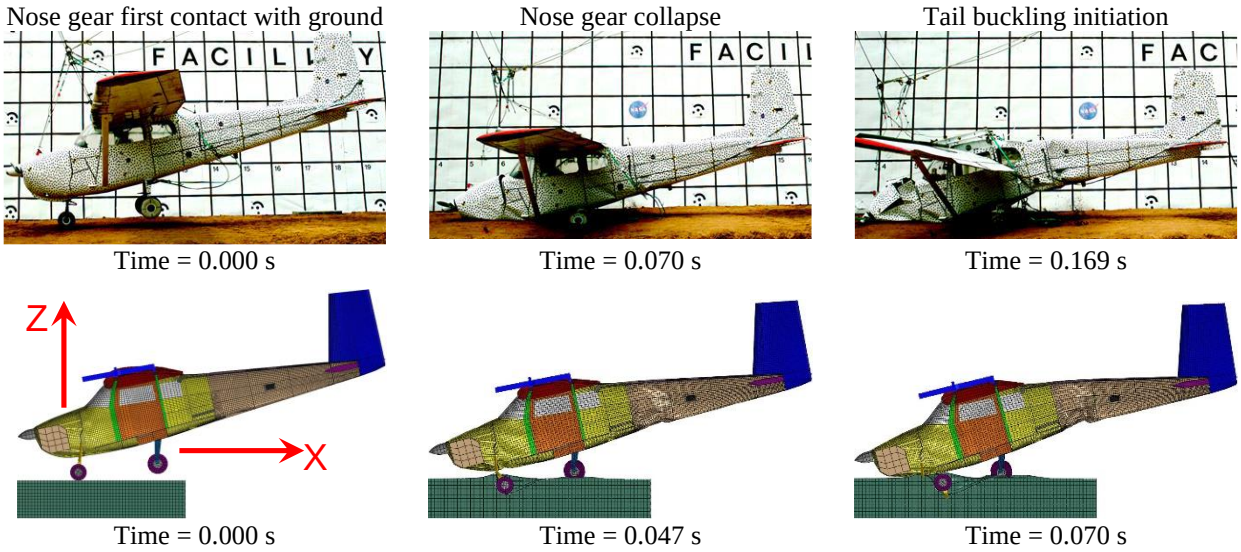

Fig. 11. Photographic images and computational models at critical kinematic events for Test 2.

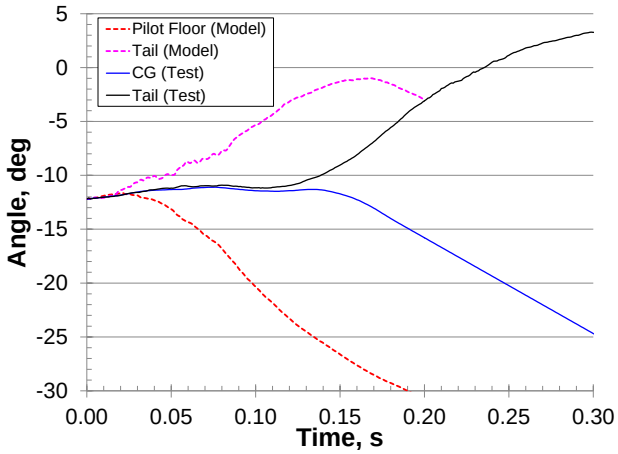

Fig. 12. Pitch angle from test and simulation against time for two locations in Test 2.

In Table 7, test and analysis comparisons of the delta-velocity, average acceleration, and peak acceleration for the horizontal (X) and vertical (Z) axes directions at several locations in the airframe are presented. Comparisons in the Z-axis direction are presented for three selected locations in the airframe (left door frame, DAS box, and rear bulkhead) in Fig. 13. Test and analytical acceleration data are filtered using an SAE CFC 20 low-pass filter and are presented in the local reference frame (moves with aircraft as shown in Fig. 3) of each accelerometer. Velocities are presented in the global coordinate system (as shown in Fig. 11).

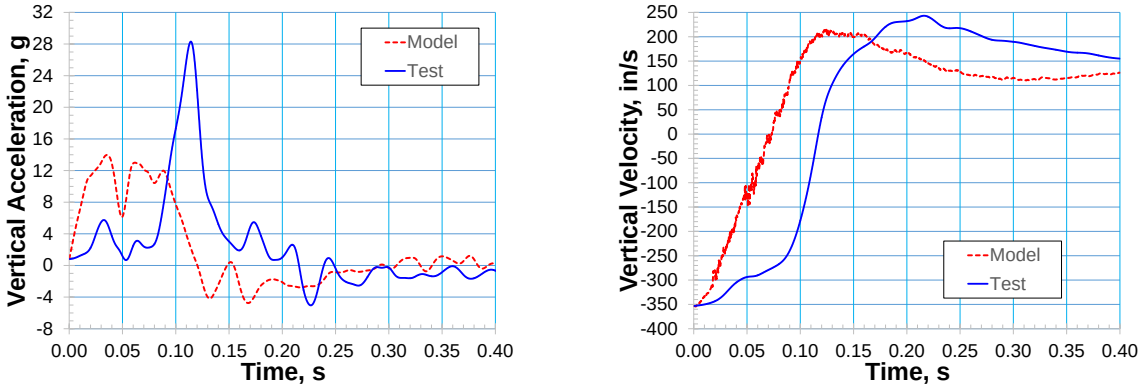

Left door frame

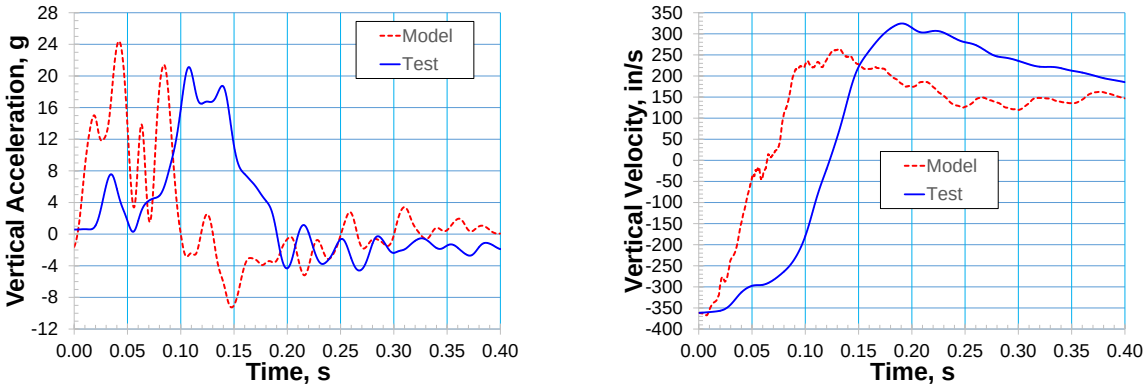

DAS box

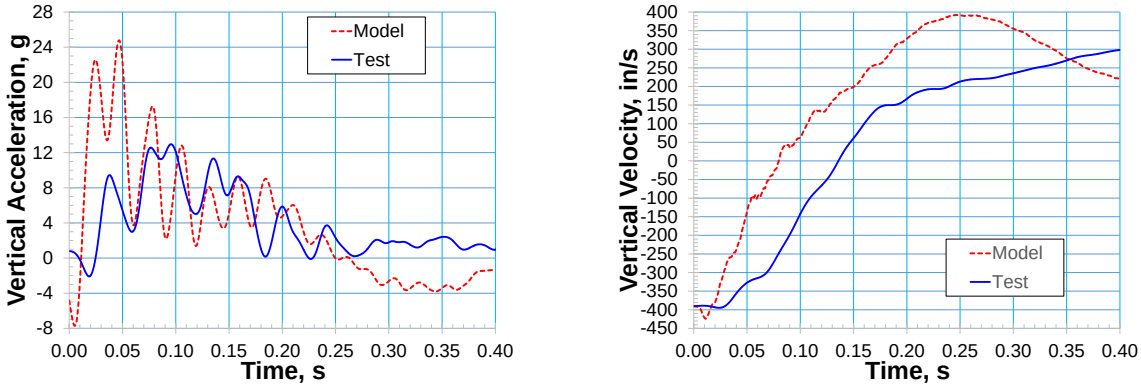

Rear bulkhead

Fig. 13. Test and analysis results of local vertical acceleration and global vertical velocity in Test 2.

Table 7. Comparison of test and analysis of velocity and acceleration at several locations for Test 2.

	Average Acceleration, g			Peak Acceleration, g			Delta-Velocity, in./s		
	Test	**Model**	**% Diff**	**Test**	**Model**	**% Diff**	**Test**	**Model**	**% Diff**
Pilot X	-9.2	-7.7	-16.2	-23.5	-21.7	-7.6	523.3	531.5	1.6
Copilot X	-9.3	-7.6	-17.9	-24.0	-20.8	-13.1	512.5	520.5	1.6
Left Door X	-9.3	-8.1	-12.9	-21.6	-18.7	-13.5	455.4	510.4	12.1
Right Door X	-6.7	-8.1	20.9	-23.5	-18.3	-22.3	421.9	511.0	21.1
DAS X	-8.8	-10.0	12.8	-33.5	-30.8	-8.1	412.9	466.5	13.0
Rear Bulkhead X	-7.6	-8.1	6.0	-15.4	-16.5	6.8	325.7	354.8	8.9
Ceiling X	-7.4	-9.5	28.2	-16.5	-18.9	14.2	319.8	373.8	16.9
Pilot Z	5.2	5.4	3.3	15.9	12.9	-19.3	475.1	518.6	9.2
Copilot Z	5.0	5.8	15.6	19.2	16.2	-15.5	444.7	504.6	13.5
Left Door Z	7.5	9.0	19.7	28.3	14.0	-50.6	583.4	570.2	-2.3
Right Door Z	8.4	8.3	-1.6	19.1	14.1	-26.0	490.9	519.1	5.7
DAS Z	9.4	8.7	-6.9	21.1	24.4	15.5	686.1	625.3	-8.9
Rear Bulkhead Z	8.5	10.9	28.0	13.0	24.8	91.3	529.9	528.5	-0.3
Ceiling Z	7.9	7.3	-7.9	24.2	17.3	-28.7	549.5	528.7	-3.8

Test and analysis comparisons of the delta-velocity and average accelerations in the airframe shown in Table 7 are good to excellent. The test and model delta-velocities were within 21% at all accelerometer locations in the airframe, with most locations below 10% difference. Comparison of the peak accelerations is good in the X direction, but good to poor in the Z direction. The test and model peak accelerations were within 23% and 29% in the horizontal and vertical directions for all but two locations in the airframe. During the test, the left door opened, but this effect is not modeled and could contribute to the 50.6% difference in peak acceleration (which is also seen in the acceleration plot in Fig. 13). Buckling in the tail section is particularly difficult to simulate as it can be significantly affected by even small imperfections in the fuselage geometry of the tail section and by the weight distribution within the tail. These uncertainties in the geometry of the tail section are likely the major contributors to the 91.3% difference in the peak acceleration. Additionally, the Mohr-Coulomb model is a relatively simple material model and may not adequately represent the soil behavior. The simple Mohr-Coulomb model may contribute to the time difference (around 0.07 sec.) in the occurrence of the acceleration and velocity peaks in Fig. 13, as described in this section of the kinematic events.

C. Crash Test 3

A sequence of photographs taken from the high-speed camera is shown in Fig. 14, along with corresponding views of the matching model kinematics. Note that the simulation model is cut in half to show the internal structure and the nose gear soil penetration. Pitch angle from photogrammetry during the test and simulation is plotted

against time in Fig. 15. The test and model pitch angle time histories match closely for the first 0.05 seconds after impact and remain within 4 degrees for the remainder of the photogrammetry data, but the tail separation angle is much more severe in the simulation. Additionally, in the simulation, the cabin section of the fuselage is not in contact with the ground at the time of tail failure as it is in the test. This delay in fuselage contact is probably due to a stiffness difference in the main landing gear, in the soil, or both. Overall, the motion of the forward fuselage in the simulation is similar to the test.

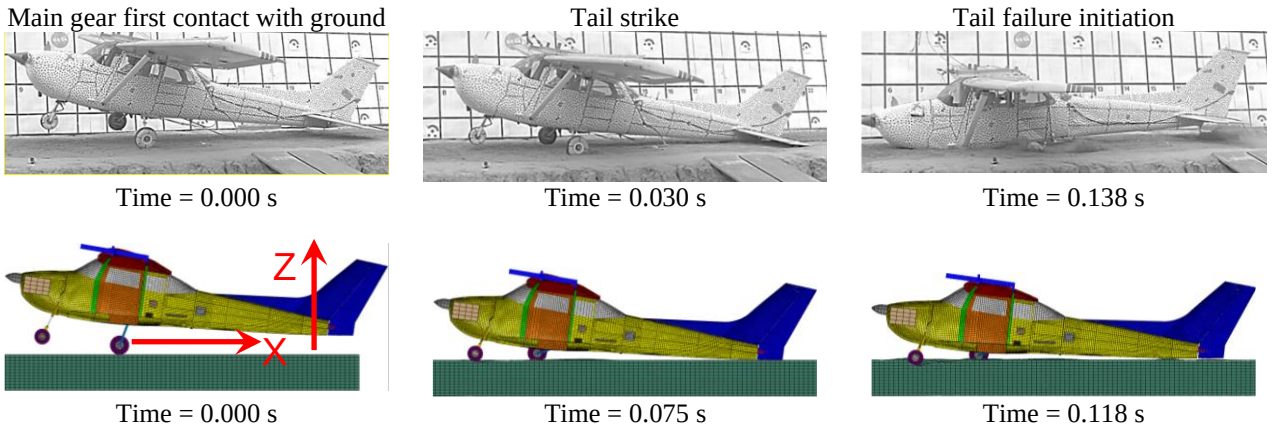

Fig. 14. Photographic images and computational models at critical kinematic events for Test 3.

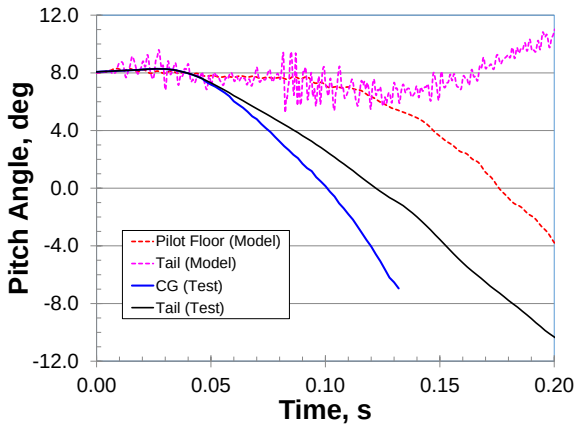

Fig. 15. Pitch angle from test and simulation against time for two locations in Test 3.

In Table 8, comparison of test and analysis results of the delta-velocity, average acceleration, and peak acceleration in the X and Z axes directions at several locations in the airframe are presented. Comparisons in the Z axis direction are presented for three selected locations in the airframe (left door frame, DAS box, and rear

bulkhead) in Fig. 16. Test and analytical acceleration data are filtered using an SAE CFC 20 low-pass filter and are presented in the local reference frame (moves with aircraft as shown in Fig. 4) of each accelerometer. Velocities are presented in the global coordinate system (as shown in Fig. 14).

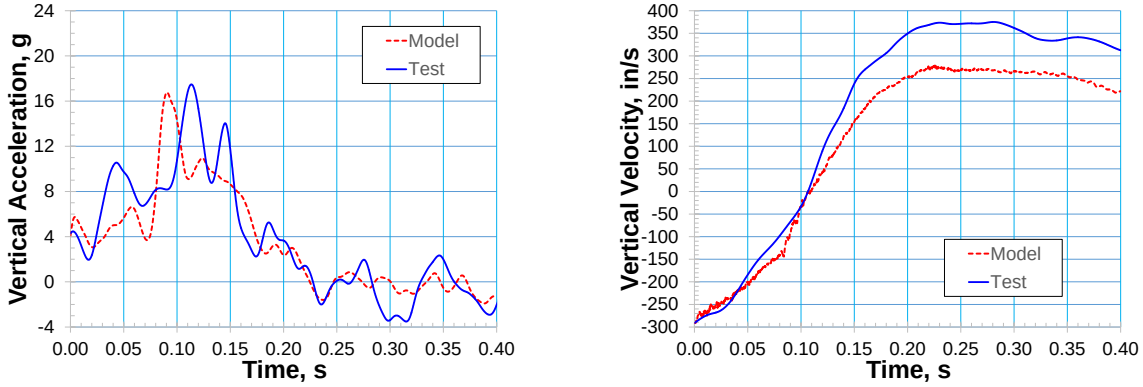

Left door frame

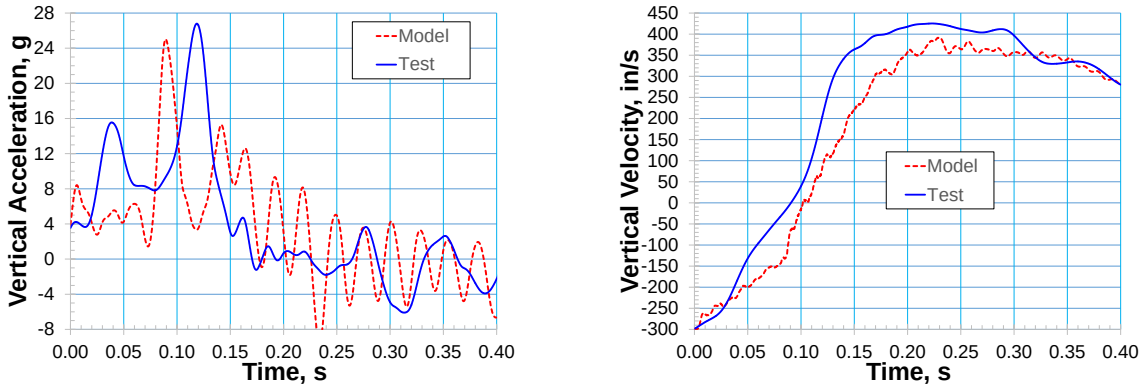

DAS box

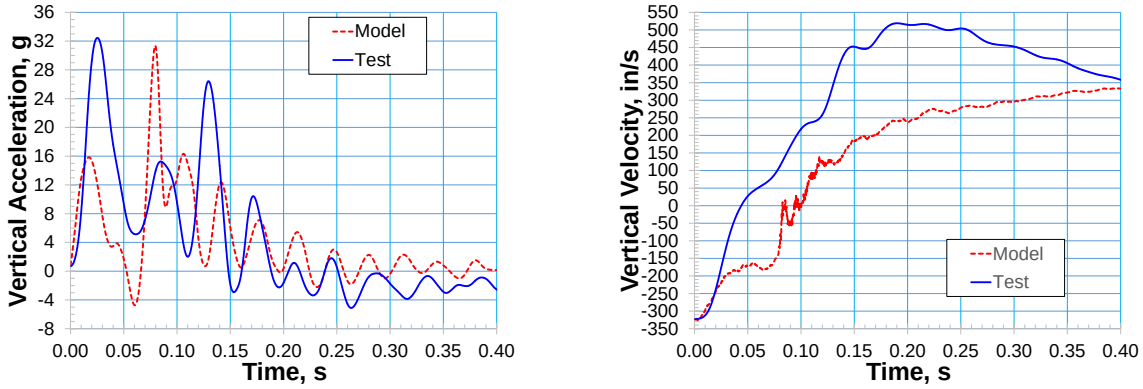

Rear bulkhead

Fig. 16. Test and analysis results of local vertical acceleration and global vertical velocity in Test 3.

Table 8. Comparison of test and analysis of velocity and acceleration at several locations for Test 3.

	Average Acceleration, g			Peak Acceleration, g			Delta-Velocity, in./s		
	Test	**Model**	**% Diff**	**Test**	**Model**	**% Diff**	**Test**	**Model**	**% Diff**
Pilot X	-5.8	-4.1	-30.1	-16.8	-10.9	-34.9	496.7	419.1	-15.6
Copilot X	-6.3	-4.0	-36.6	-16.6	-10.7	-35.6	504.0	418.7	-16.9
Left Door X	-5.3	-3.6	-31.4	-14.9	-10.9	-27.0	467.4	390.1	-16.5
Right Door X	-5.5	-3.8	-30.3	-13.9	-11.1	-20.0	437.8	390.9	-10.7
DAS X	-5.2	-3.4	-33.2	-14.1	-12.1	-13.9	365.5	363.0	-0.7
Rear Bulkhead X	-4.4	-3.4	-22.9	-11.5	-12.0	5.0	319.7	348.3	8.9
Ceiling X	-4.0	-2.1	-48.4	-9.4	-7.7	-17.9	255.3	234.6	-8.1
Firewall X	-6.5	-3.5	-45.7	-22.0	-9.6	-56.5	284.2	295.2	3.9
Pilot Z	6.0	5.2	-13.0	16.6	13.5	-18.3	572.0	483.5	-15.5
Copilot Z	5.7	4.8	-16.3	15.7	14.1	-10.1	527.7	483.5	-8.4
Left Door Z	7.6	6.5	-14.5	17.5	16.8	-4.1	664.5	570.2	-14.2
Right Door Z	6.8	6.6	-4.0	20.2	16.4	-18.6	664.2	569.5	-14.3
DAS Z	8.1	7.1	-12.4	26.8	25.0	-6.6	723.7	690.3	-4.6
Rear Bulkhead Z	9.2	7.4	-19.7	32.5	31.4	-3.4	842.2	574.9	-31.7
Ceiling Z	6.3	6.3	0.8	19.8	21.0	6.2	598.1	555.3	-7.2
Firewall Z	6.6	5.0	-23.8	14.2	12.3	-13.5	357.9	335.2	-6.3

Test and analysis comparisons of the delta-velocities in the airframe shown in Table 8 are good to excellent (within 17%) except in the tail due to the large damage that occurs there. The poor correlation in the tail is also seen in the delta-velocity plot in Fig. 16. Correlation of the average and peak accelerations is good to excellent in the Z direction except at the damaged firewall (24%). Also, note that in Fig. 16 timing of the acceleration and velocity peaks in the Z direction from the simulation and the test are close (within around 0.02 sec). In Table 8, correlation of the average and peak accelerations in the X direction is poor, probably because of the delay in the fuselage impact with the ground as described in the previous discussion of the kinematic events. The delay in the simulation results in a reduction of the time that the belly of the fuselage is in contact with the soil, and hence, a reduction in the horizontal deceleration due to friction between the fuselage and the soil. The delay could be due to uncertainty of the stiffness of the landing gear and uncertainty in definition of the zero-degree pitch angle of the model and the test article. Additionally, the Mohr-Coulomb model is a relatively simple material model and may not adequately represent the soil behavior.

Summaries of the comparison of test and analysis results of vertical delta-velocity and vertical acceleration at three airframe locations (left door frame, DAS box, and rear bulkhead) for all three tests are presented in Tables 9 and 10, respectively.

Table 9. Test and analysis comparisons of vertical delta-velocity.

Location	% Difference		
	Test 1	Test 2	Test 3
Left Door Frame	2.1	-2.3	-14.2
DAS Box	-2.6	-8.9	-4.6
Rear Bulkhead	-2.2	-0.3	-31.7

Table 10. Test and analysis comparisons of peak vertical acceleration.

Parameter	% Difference		
	Test 1	Test 2	Test 3
Left Door Frame	27.4	-50.6	-4.1
DAS Box	27.4	15.5	-6.6
Rear Bulkhead	38.7	91.3	-3.4

IV. Mesh Refinement and Parametric Studies

Results from the numerical FE models described in this paper are affected by numerous uncertainties. These uncertainties include material thicknesses in components that could not be easily measured, uncertainties in impact surface conditions, and numerical uncertainties due to effects of finite element mesh size. In this section, a mesh convergence study is conducted and the effects of several key parameters on the numerical response of the Cessna model are described.

A. Numerical Mesh Convergence

The internal structures of all three FE models were similar. As shown in Fig. 17, the fuselage frames, wing spars, wing ribs, empennage spars, and empennage ribs were modelled with shell elements. In most components of the FE model, a minimum of three shell elements were used to properly represent the bending shape of the structure. In the fuselage frames and stringers, this minimum of three elements is used in the mesh. In the ribs and spars, four elements were used. In the wing cover panels and fuselage panels, significantly more elements are used (typically eight to twenty elements). Adequate mesh refinement was desired in regions that were critical to the deformation response of the aircraft (such as the landing gear) and regions that contained accelerometers (such as the bulkheads). A formal mesh convergence study for an entire Cessna FE model was not performed, but mesh refinements of the landing gear support and aft bulkhead, shown in Figs. 18 and 19, respectively, were performed. In the refined meshes, the element size was cut in half in both directions. Only the responses due to Test 1 landing conditions were studied.

In Fig. 20, the effect of the mesh refinement on the pitch response and accelerations in the vertical coordinate system are shown. The shapes and peaks of the pitch angle responses and accelerations for the refined mesh are very close to the baseline responses. In Table 11, the maximum pitch angle and peak vertical acceleration for the refined meshes are within 1.4% and 3.5%, respectively of the baseline values, so the baseline mesh is considered to be converged.

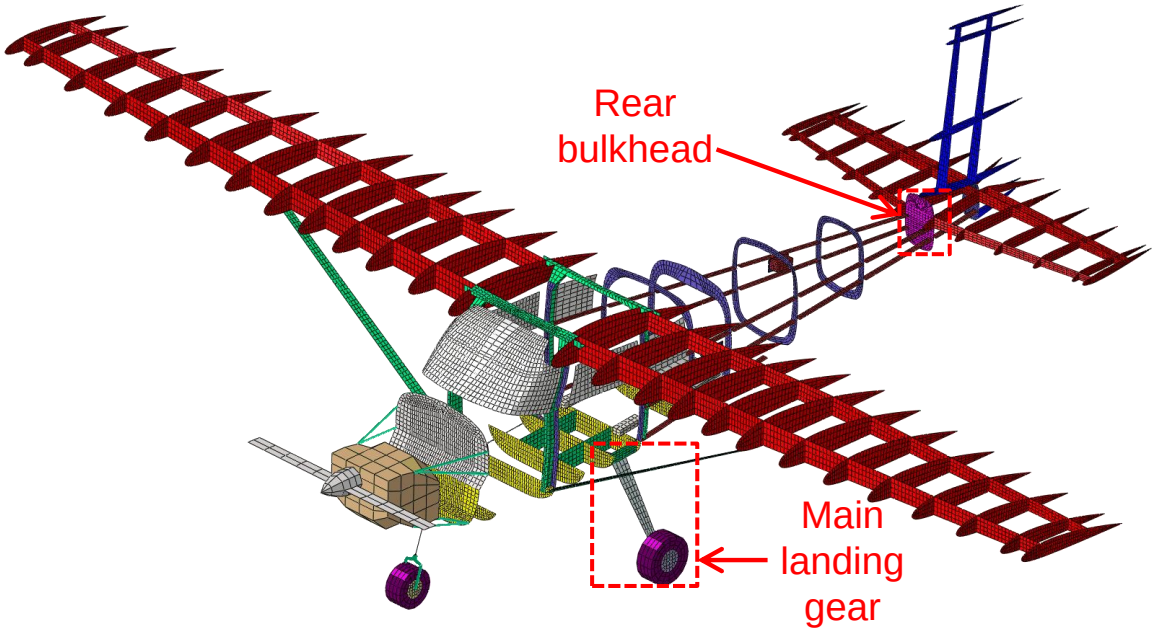

Fig. 17. Internal structure of the FE model of the C-172 airframe (Test 1 and 2).

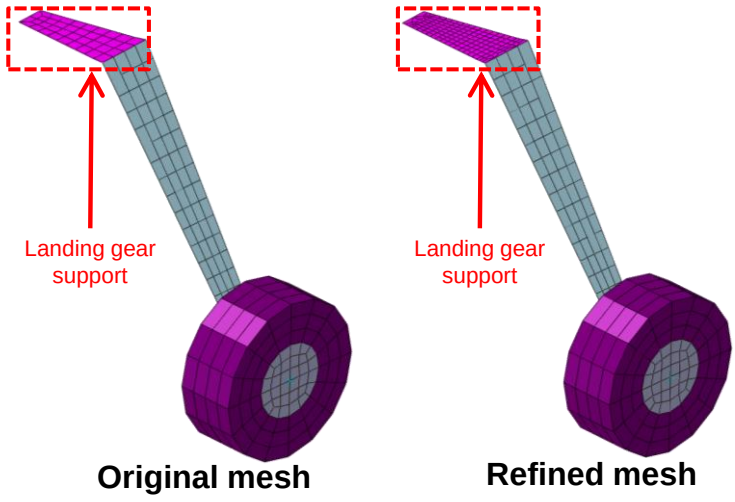

Fig. 18. Mesh refinement of landing gear support component.

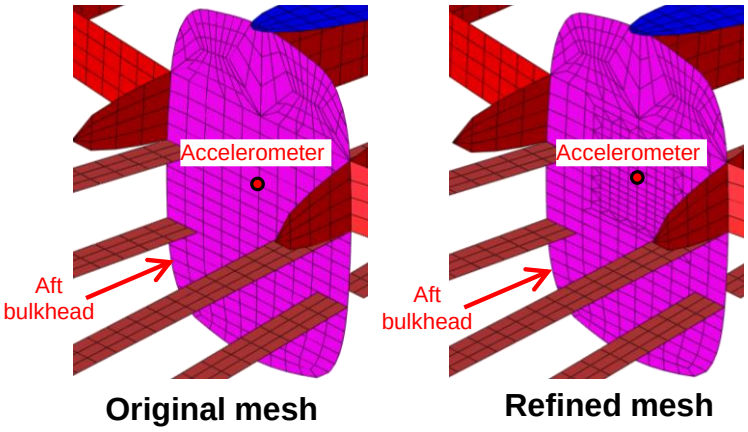

Fig. 19. Mesh refinement of aft bulkhead component.

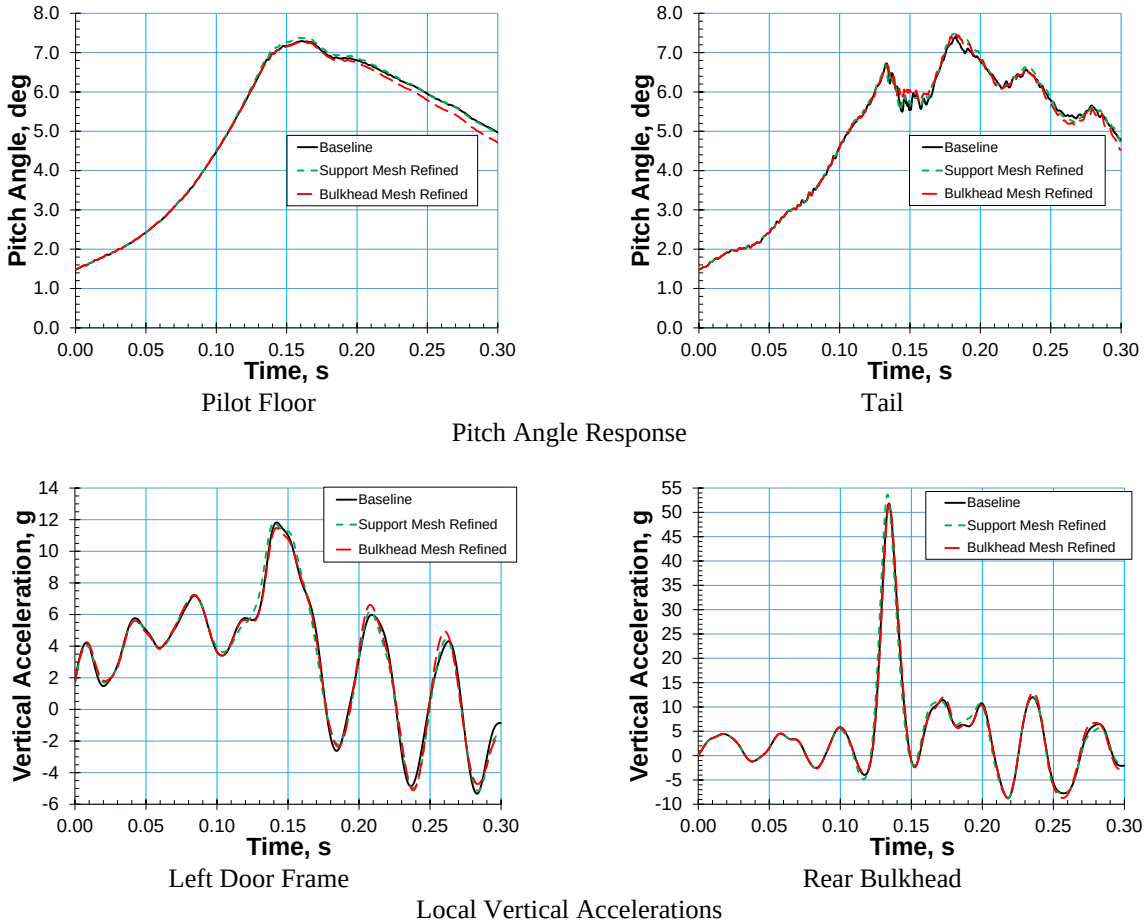

Fig. 20. Sensitivity of pitch angle response and local vertical acceleration due to mesh refinement.

Table 11. Comparison of pitch response and accelerations of baseline and refined meshes

Parameter	% Difference for Refined Support Mesh	% Difference for Refined Bulkhead Mesh
Pitch Angle at Pilot Floor	1.2	-0.3
Pitch Angle at Tail	1.4	0.9
Acceleration at Left Door Frame	0.2	-2.9
Acceleration at Rear Bulkhead	3.5	-0.2

B. Parametric Studies

Several types of uncertainties affect the test and numerical results in this paper. Test results are subject to uncertainties in the measurement equipment and data processing. To deal with these uncertainties, the accelerometers used in the tests were calibrated to an accuracy of 1% of reference input. No other uncertainty data are available for the test setup. The numerical models are subject to modelling uncertainties, i.e., differences between the physical test specimens and the numerical representation of those specimens. To evaluate the sensitivity of the numerical results to some of these modelling uncertainties, a series of parametric studies were conducted to evaluate the effects of three key model parameters: friction between the ground and the tires, thickness in the main landing gear strut support, and thickness of the aft bulkhead.

In Fig. 21, the sensitivity of the pitch response and accelerations in the vertical coordinate system to reduction in ground friction and increases in the main landing gear support and rear bulkhead thicknesses are shown. When the ground friction is reduced, the landing gear tend to spread outward (in the Y direction) more, resulting in a slightly lower maximum pitch angle and an increase in accelerations at the pilot floor and in the tail section. A 10% increase in the thickness of the support structure for the landing gear has the opposite effect, making the landing gear a stiffer spring, delaying the rebound response of the vehicle, and significantly reducing the accelerations. A 20% increase in the thickness of the rear bulkhead reduced the pitch angle response by less than 2% and reduced the accelerations by less than 4%. According to Table 12, the increase in the thickness of the landing gear support structure had the greatest effect on the structural response, with a 10% increase in pitch angle and 28.6% decrease in accelerations in the tail section.

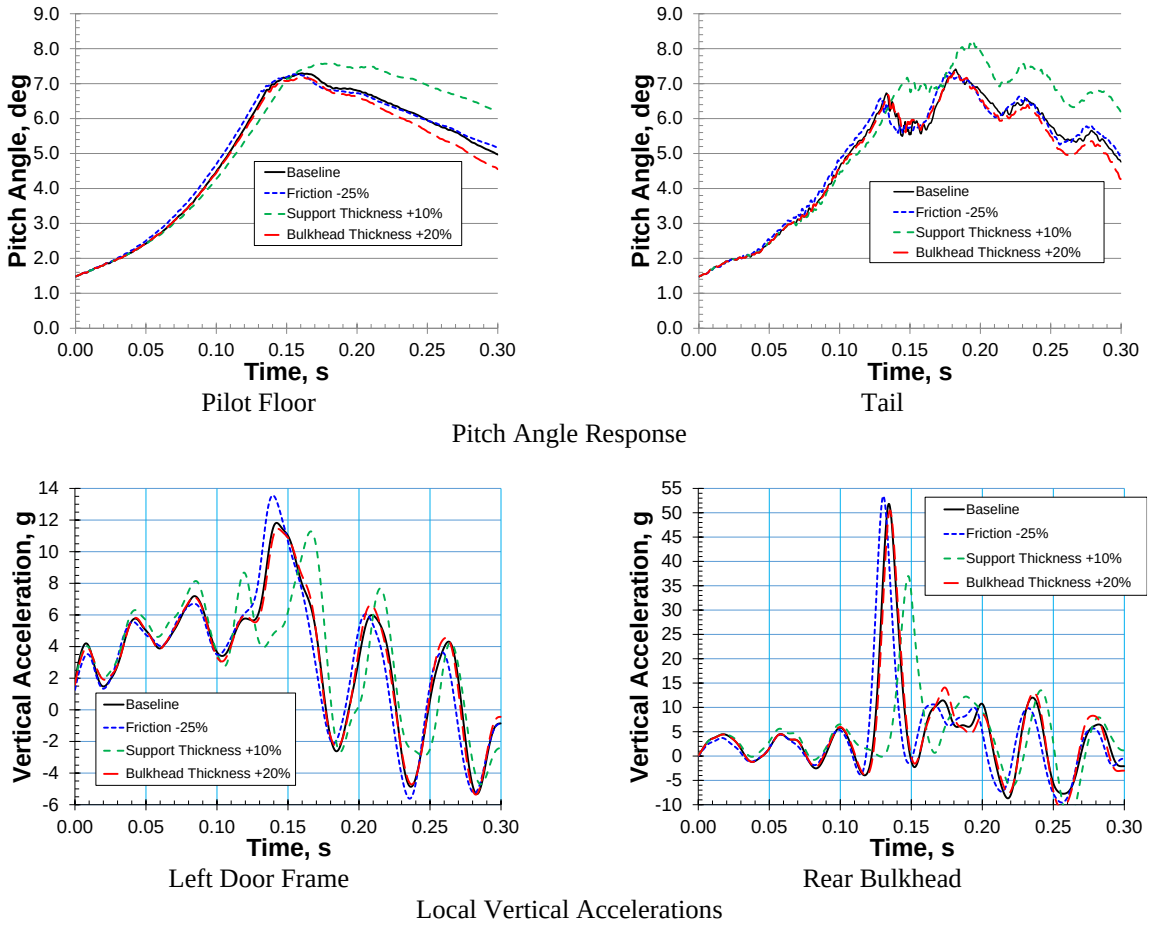

Fig. 21. Sensitivity of pitch angle response and local vertical acceleration to changes in friction and thicknesses.

Table 12. Sensitivity of pitch response and accelerations to friction and thickness changes.

Parameter	% Change Due to Decrease in Friction	% Change Due to Increase in Support Thickness	% Change Due to Increase in Bulkhead Thickness
Pitch Angle at Pilot Floor	-0.3	3.9	-1.6
Pitch Angle at Tail	-1.2	10.0	-0.9
Acceleration at Left Door Frame	14.7	-4.6	-3.2
Acceleration at Rear Bulkhead	3.0	-28.6	-2.6

V. Concluding Remarks

Test data from three full-scale aircraft impact tests and corresponding computer simulations analyzed using the Abaqus explicit FE software are presented in this paper. An advanced modeling tool was used to generate a complete FE model from a combination of planform dimensions and a series of manual measurement of the test aircraft. The predictive model required only minor calibration once the test data was captured. The calibrated

model was obtained by making small adjustments to non-structural masses and modifying the landing gear stiffnesses to match the physical properties of the actual test aircraft.

Comparisons of test and analysis data included inertial properties, time histories of airframe motion (pitch angle), and time histories of velocities and accelerations. The overall findings of the study are:

1) Total weight of the models matched the test articles within 0.001%, and the CG locations matched within 0.4%, which is considered excellent agreement.
2) Kinematic responses of the model were similar to the tests, although a time shift in the response was noted, probably due to uncertainties in the soil properties.
3) Delta velocities of the model and test were within 10% for the majority of the airframe locations in all tests.
4) Peak accelerations for the model were usually within 20% to 40% of the values for the test except at the tail and firewall which were damaged in Tests 2 and 3.
5) Uncertainties in weight distribution, unmodeled components, and soil properties contributed to most of the discrepancies between test and analysis.
6) Damage to the aircraft fuselage occurred immediately aft of the cabin section in all three crash scenarios; consequently, the wires connecting the ELT to the antenna should not cross this axial position in the aircraft. Installation of the ELT and its antenna in close proximity to each other minimizes the risk that the connecting wires are routed through an area that can experience severe damage, thus compromising the connection.
7) Mounting an ELT in a location subject to very large accelerations at lower impact velocities (such as the rear bulkhead) should be avoided to prevent activation of the ELT during minor incidents, such as a runway bump.
8) Mesh refinement resulted in a small (3.5%) change in peak accelerations, so the model is considered to be converged.
9) A parameter study was used to demonstrate that the response of the aircraft model is very sensitive to the thickness of the landing gear support structure (with a 28.6% increase in peak acceleration from a 10% change in thickness), and is much less sensitive to the thickness of the aft bulkhead and soil friction.

Due to the excellent correlation between analysis and test, the simulation models are suitable for further studies evaluating alternative ELT mounting configurations and for evaluating airframe performance under different impact conditions.

V. Funding Sources

The authors of this paper are employed by the National Aeronautics and Space Administration (NASA), and the research presented in this paper was directly funded by the U. S. Government.

VI. References

1 Federal Aviation Administration, "Installation and Inspection Procedures for Emergency Locator Transmitters and Receivers," Federal Aviation Administration Advisory Circular, AC No. 91-44A, February 2018. https://www.faa.gov/documentLibrary/media/Advisory_Circular/AC_91-44A_CHG-1.pdf

2 NASA, "NASA's Gantry: Past, Present and Future Asset to Exploration." http://www.nasa.gov/centers/langley/news/factsheets/fs-2007-08-138-larc.html.

3 Vaughan Jr., V. L., and Alfaro-Bou, E., "Impact Dynamics Research Facility for Full-Scale Aircraft Crash Testing," NASA Technical Note TN-D-8179, April 1976.

4 Littell, J. D., "Crash Tests of Three Cessna 172 Aircraft at NASA Langley Research Center's Landing and Impact Research Facility," NASA Technical Memorandum TM-2015-218987, November 2015.

5 Castle, C. B., and Alfaro-Bou, E., "Light Airplane Crash Tests at Three Flight-Path Angles," NASA Technical Paper TP-1210, June 1978.

6 Hayduk, R. J., "Comparative Analysis of PA-31-350 Chieftain (N44LV) Accident and NASA Crash Test Data," NASA Technical Memorandum TM-80102, October 1979.

7 Castle, C. B., and Alfaro-Bou, E., "Light Airplane Crash Tests at Three Roll Angles," NASA Technical Paper TP-1477, October 1979.

8 Vaughan Jr., V. L., and Alfaro-Bou, E., "Light Airplane Crash Tests at Three Pitch Angles," NASA Technical Paper TP-1481, November 1979.

9 Vaughan Jr., V. L., and Hayduk, R. J., "Crash Tests of Four Identical High-Wing Single Engine Airplanes," NASA Technical Paper TP-1699, August 1980.

10 Alfaro-Bou, E., Williams, M. S., and Fasanella, E. L., "Determination of Crash Test Pulses and Their Application to Aircraft Seat Analysis," Society of Automotive Engineers SAE-810611, 1981, https://doi.org/10.4271/810611.

11 Williams, M. S., and Fasanella, E. L., "Crash Tests of Four Low-Wing Twin-Engine Airplanes with Truss-Reinforced Fuselage Structure," NASA Technical Paper TP-2070, September 1982.

12 Carden, H. C., "Correlation and Assessment of Structural Airplane Crash Data with Flight Parameters at Impact," NASA Technical Paper TP-2083, November 1982.

13 Melosh, R. J. and Kamat, M. P., "Computer Simulation of Light Aircraft Crash," *Journal of Aircraft*, Vol. 14, No. 10, October 1977, https://doi.org/10.2514/3.44631.

14 Code of Federal Regulations - Title 14: Aeronautics and Space, Part 23: Airworthiness Standards: Normal, Utility, Acrobatic, and Commuter Category Airplanes, 23.562 - Emergency landing dynamic conditions.

15 Jackson, K. E., Boitnott, R. L., Fasanella, E. L., Jones, L. E., and Lyle, K. H., "A History of Full-Scale Aircraft and Rotorcraft Crash Testing and Simulation at NASA Langley Research Center," NASA Technical Memorandum TM-2004-0191337, January 2004.

16 Hurley, T. R. and Vandenburg, J. M., editors, "Small Airplane Crashworthiness Design Guide," AGATE Report Reference No. AGATE-WP3.4-034043-036, Simula Technologies Reference No. TR-98099, April 2002.

17 Jackson, K. E. and Fasanella, E. L., "NASA Langley Research Center Impact Dynamics Research Facility Research Survey," *Journal of Aircraft*, Vol. 41, No. 3, pp. 511-522, May 2004, https://doi.org/10.2514/1.3082.

18 Thomson, R. G., and Goetz, R. C., "NASA/FAA General Aviation Crash Program – A Status Report," *Journal of Aircraft*, Vol. 17, No. 8, pp. 584-590, August 1980, https://doi.org/10.2514/3.57943.

19 Wittlin, G., "Analysis of Aircraft Dynamic Behavior in a Crash Environment," *Journal of Aircraft*, Vol. 20, No. 9, pp. 762-769, September 1983, https://doi.org/10.2514/3.44940.

20 McComb, Jr., H. G., Thomson, R. G., Hayduk, R. J., "Structural Dynamics Research in a Full-Scale Transport Aircraft Crash Test," *Journal of Aircraft*, Vol. 24, No. 7, pp. 447-453, July 1987, https://doi.org/10.2514/3.45500.

21 Thomas, M., Chitty, D., Gildea, M., and T'Kindt, C., "Constitutive Soil Properties for Unwashed Sand and Kennedy Space Center," NASA Contractor Report CR-2008-215334, July 2008.

22 Annett, M. S., Little, J. D., Jackson, K. E., Bark, L. W., DeWeese, R. L., and McEntire, B. J., "Evaluation of the First Transport Rotorcraft Airframe Crash Testbed (TRACT 1) Full-Scale Crash Test," NASA Technical Memorandum TM-2014-218543, October 2014.

23 Annett, M. A., Littell, J. D., Stimson, C. M., Jackson, K. E., and Mason, B. H., “Full-Scale Crash Tests and Analyses of Three High-Wing Single Engine Aircraft,” Aerospace Structural Impact Dynamics International Conference, Seville, Spain, November 17-19, 2015.

24 Jackson, K. E. and Fasanella, E. L., “Crash Testing and Simulation of a Cessna 172 Aircraft: Hard Landing onto Concrete,” 14th International LS-DYNA Users Conference, Dearborn, MI, June 13-14, 2016.

25 Fasanella, E. L. and Jackson, K. E., “Crash Testing and Simulation of a Cessna 172 Aircraft: Pitch Down Impact onto Soft Soil,” 14th International LS-DYNA Users Conference, Dearborn, MI, June 13-14, 2016.

26 Mason, B. H. and Quinlan, J. R., "Conceptual Design Shop: A Tool for Rapid Airframe Structural Modeling," AIAA 2018-2001, 59th AIAA/ASCE/AHS/ASC SDM Conference, Kissimmee, FL, January 8-12, 2018, https://doi.org/10.2514/6.2018-2001.

27 PATRAN 2016 Release Guide, MSC Software, MSC Software, Santa Ana, CA 92707.

28 Abaqus, *Abaqus User’s Manual*, Vol III, Version 6.14, Dassault Systèmes Simulia Corp., Pawtucket, RI, 2012.

29 Society of Automotive Engineers (SAE), “Recommended Practice: Instrumentation for Impact Test – Part 1,” Electronic Instrumentation, SAE J211-1, March 1995.